ChemPubSoc Europe

DOI: 10.1002/chem.201801022

CHEMISTRY A European Journal Full Paper

Lipid Bioimaging

Synthesis and Self-Assembly of Bay-Substituted Perylene Diimide Gemini-Type Surfactants as Off-On Fluorescent Probes for Lipid Bilayers

Jurgen Schill,[a] Sam van Dun,[a] Maarten J. Pouderoijen,[b] Henk M. Janssen,[b] Lech-Gustav Milroy,[a] Albertus P. H. J. Schenning,*[c] and Luc Brunsveld*[a]

Abstract: Interest in bay-substituted perylene-3,4:9,10-tetracarboxylic diimides (PDIs) for solution-based applications is growing due to their improved solubility and altered optical and electronic properties compared to unsubstituted PDIs. Synthetic routes to 1,12-bay-substituted PDIs have been very demanding due to issues with steric hindrance and poor regioselectivity. Here we report a simple one-step regioselective and high yielding synthesis of a 1,12-dihydroxylated PDI derivative that can subsequently be alkylated in a straightforward fashion to produce nonplanar 1,12-dialkoxy PDIs. These PDIs show a large Stokes shift, which is specifically useful for bioimaging applications. A particular cationic PDI gemini-type surfactant has been developed that forms nonfluorescent self-assembled particles in water ("off state"), which exerts a high fluorescence upon incorporation into lipophilic bilayers ("on state"). Therefore, this probe is appealing as a highly sensitive fluorescent labelling marker with a low background signal for imaging artificial and cellular membranes.

Introduction

Substituted perylene-3,4:9,10-tetracarboxylic diimides (PDIs) have attracted interest for a variety of applications, including organic electronics,[1–3] single molecule spectroscopy[4–6] and bioimaging.[7–9] For bioimaging, fluorescent quenching of PDIs has been used to sense hydrophobicity changes such as in artificial and cellular bilayers.[10–20] However, PDIs as highly sensitive fluorescent probes with a low background signal are still rare. Such off-on fluorescent probes would be appealing for cellular imaging. Also, surprisingly few examples have been reported of water-soluble PDIs not bearing large-MW solubilising substituents (e.g., dendrimer like).[9,21–23]

Fine tuning of the physical, optical, and electronic properties of PDIs is typically achieved through substitution of the perylene ring system at either the imide-, *ortho*-, or bay positions, or a combination of the three to customise the optical, electronic and self-assembly properties of the PDIs (Figure 1 a).[24,25] Substituents on the imide nitrogen atoms of PDIs tend to im-

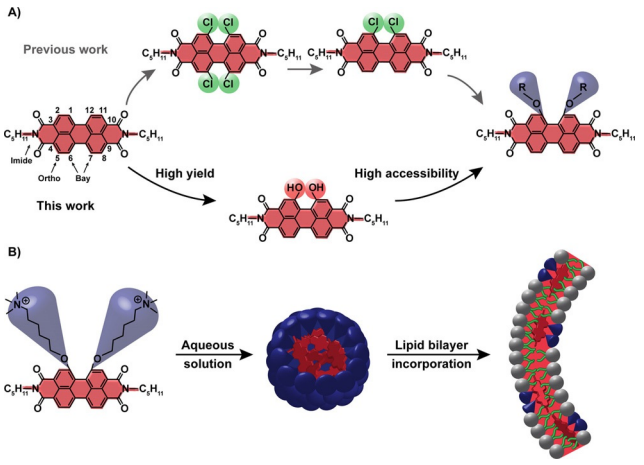

Figure 1. Schematic overview of A) the synthesis approach from previous work through multistep halogenation and dehalogenation, which is typically low yielding. The novel approach presented here involves direct dihydroxylation of a single-side bay. B) The self-assembly of a cationic PDI derivative into nanostructures and the incorporation of these PDI molecules into lipophilic bilayers for bioimaging.

[a] J. Schill, S. van Dun, Dr. L.-G. Milroy, Prof. Dr. L. Brunsveld
Laboratory of Chemical Biology, Department of Biomedical Engineering and Institute for Complex Molecular Systems, Eindhoven University of Technology, P.O. Box 513, 5600MB Eindhoven (The Netherlands)
E-mail: l.brunsveld@tue.nl

[b] M. J. Pouderoijen, Dr. H. M. Janssen
SyMO-Chem B.V., Den Dolech 2, 5612AZ Eindhoven (The Netherlands)

[c] Prof. Dr. A. P. H. J. Schenning
Stimuli-responsive Functional Materials and Devices and Institute for Complex Molecular Systems, Eindhoven University of Technology
P.O. Box 513, 5600MB, Eindhoven (The Netherlands)
E-mail: a.p.h.j.schenning@tue.nl

Supporting information and the ORCID identification numbers for the authors of this article can be found under: https://doi.org/10.1002/chem.201801022.

prove solubility[26,27] while retaining the planarity of the perylene aromatic ring system, thus preserving the perylene's optical properties.[28] N-substitution of PDIs can also influence their self-assembly properties, which has stimulated intensive studies into bulk and solution-based applications of these compounds.[29–32] By contrast, substitution of the perylene ring system at either the *ortho*- or bay positions can significantly influence the optical and solubility properties of the PDIs, dependent upon the substitution pattern, the steric bulk and electronic properties of the substituent group.[33–36] Bay substitution, for example, increases steric hindrance in this region of the molecule, which is relieved by out-of-plane twisting of the PDIs perylene ring system. This phenomenon causes a disruption to the π–π stacking behaviour of the PDI, which leads to improved solubility and altered physical properties.[33,37] Substitution of PDIs at the bay position is, however, synthetically demanding, involves halogenation reactions, and predominantly four-fold bay-substituted PDIs have been reported.[35,38–43] Partly substituted 1,6- and 1,7-regioisomers, commonly as mixtures,[44–48] have also been synthesised,[49,50] while 1,12-bay-substituted PDIs have been rarely reported. The latter are interesting because the distortion of the perylene ring system by the 1,12-substitution will strongly alter the optical properties of the compound, comparable to their corresponding tetrasubstituted PDIs, while solubility and self-assembly properties will be different.[51–53] Unfortunately, 1,12-bay-substituted PDIs have to be accessed through halogenation/dehalogenation chemistry,[54–57] which is typically inefficient, cumbersome, and low yielding. Controlled and efficient access to 1,12-bay-substituted PDIs is evidently challenging, and yet also potentially highly valuable given their untapped chemical potential and prospective influence on the PDIs optical properties.

Here we report a one-step, atom-efficient, and regioselective synthesis of a 1,12-dihydroxylated PDI based on violanthrone chemistry (Figure 1 a).[58] This bay-substituted PDI acts as an intermediate towards the introduction of structurally diverse polar and apolar side-chains through straightforward O-alkylation chemistry. A particular cationic bay-substituted PDI derivative, resulting from this synthetic approach, can be regarded as a new type of gemini-surfactant[59] bearing two hydrophilic head groups, two hydrophobic groups and a rigid fluorescent core. This amphiphile forms nonfluorescent self-assembled particles in aqueous solution and lights up upon incorporation in a hydrophobic matrix. This property can be exploited as an off-on fluorescence probe for artificial and cellular lipid bilayers (Figure 1 b).

Results and Discussion

Starting material PDI **1** was prepared from parent perylene-3,4:9,10-tetracarboxylic dianhydride and *n*-amylamine[60] and purified[61] according to reported procedures. Using a procedure derived from violanthrone chemistry,[58] PDI **1** was subsequently oxidised by activated manganese(IV) oxide (MnO_2) in sulfuric acid and then partially reduced using sodium sulfite, introducing two hydroxyl groups at positions 1 and 12, yielding PDI **2** (Scheme 1). The ^{1}H and ^{13}C NMR of PDI **2** was found to be remarkably clean. Moreover, a broad vibrational mode associated with OH stretching was observed for PDI **2** in the functional group region of the solid-phase infrared spectrum, providing further evidence for the introduction of the hydroxyl groups (Figure S1). Given its low solubility, PDI **2** was directly used for alkylation without further purification. Substitution of the bay hydroxyls were chosen such that PDI derivatives with varying side-chain polarity were synthesised. This allows for a clear analysis of the influence of side-chain polarity on the photophysical and morphological properties of the products. With 1,12-dihydroxylated PDI **2** in hand, subsequent reactions with 2-ethylhexylbromide, monomethyl triethylene glycol *p*-toluenesulfonate, 1,6-dibromohexane and *n*-octylbromide yielded PDI **3**–**5** and **7**, respectively (Scheme 1). Notably, all introduced

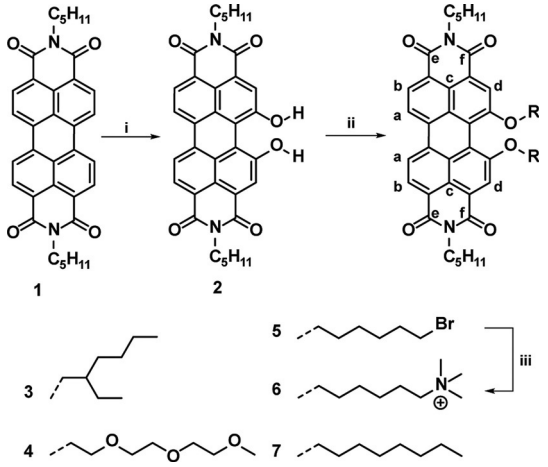

Scheme 1. Direct 1,12-dihydroxylation of the perylene-3,4:9,10-tetracarboxylic diimides (PDIs) and subsequent synthetic route to PDI **3**–**7**. i) H_3BO_3, MnO_2, H_2SO_4, room temperature, 16 h, quant; ii) K_2CO_3 or DIPEA, dimethylformamide, 100 °C, 48 h, 43 % (**3**), 60 % (**4**), 43 % (**5**) and 13 % (**7**); iii) trimethylamine, tetrahydrofuran, room temperature, 24 h, quant.

linear and branched bay substituents ensured excellent solubility of PDI **3**–**5** and **7** in organic solvents as compared with the solubilities of their parent PDIs **1** and **2**. After separation of PDI **5** from its cyclised side product by silica gel chromatography, substitution of the bromides with trimethylamine yielded doubly charged cationic species PDI **6**, which was conveniently purified by precipitation from acetone. As discussed previously, substitution at bay area positions, such as the 1,12-positions, can be particularly challenging because of steric restrictions. In contrast, this synthetic route has allowed for satisfactory overall yields of 43, 60, 43 and 13 % for PDI **3**–**5** and **7**, respectively.

Examination of PDI **2** revealed no evidence for the formation of mono-, tri- or tetra-bay hydroxylated derivatives by mass spectrometry, ^{1}H and ^{13}C NMR analyses. Considering the much improved solubility of the substituted derivative of PDI **2**, a detailed 2D-NMR study was performed on PDI **3** (Figures S2–S5 in the Supporting Information). The perylene-bound protons of PDI **3** were assigned by the presence of $^3J_{CH}$ correlations between protons H_b ($\delta = 8.55$ ppm) and carbonyl carbons C_e ($\delta =$ 163.9 ppm) and between H_d ($\delta = 8.43$ ppm) and carbonyl car-

bons C_f ($\delta = 163.8$ ppm) and by the absence of this correlation for H_a ($\delta = 8.48$ ppm) (Figure 2a). The presence of additional $^3J_{CH}$ correlations between protons H_b ($\delta = 8.55$ ppm) and H_d ($\delta = 8.43$ ppm) with carbon C_c ($\delta = 123.6$ ppm) and the absence of a $^3J_{CH}$ correlation between one single carbon both with H_a ($\delta = 8.48$ ppm) and H_d ($\delta = 8.43$ ppm) simultaneously, is consistent with either a 1,7- or a 1,12-substituted[56] isomer. Protons H_g were observed as two signals at $\delta = 4.28$ and 4.02 ppm, both correlating with a single carbon signal C_g at $\delta = 72.8$ ppm in a HSQC experiment (Figure S3). Cross peaks between these proton signals were observed in a COSY experiment (Figure S4), indicating that each signal arises from two protons H_g, each bound to a different C_g carbon, and that protons H_g are thus diastereotopic. In a NOESY experiment, these protons show a through-space dipolar interaction with protons H_d, corroborating the 1,12-substitution topology. Moreover, cross peaks between protons H_g were herein also observed, which is expected for nonequivalent protons bound to the same carbon (Figure S5). However, these nonexchangeable protons show the same phase as the diagonal, indicating conformational exchange, classified as restricted rotation, at these positions.[62] These conformational exchange peaks lead to the assumption that the 1,12-substitution pattern distorts the aromatic ring system of the perylene, hence altering the physical properties as noted before herein.

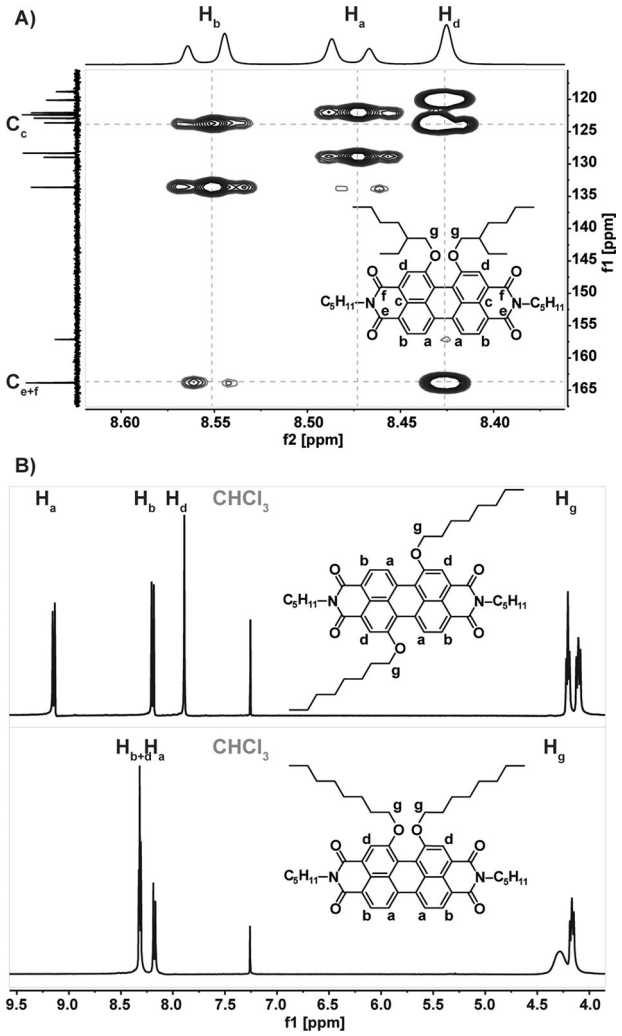

Figure 2. A) Expansion of the aromatic region of the 2D ^{1}H, ^{13}C HMBC spectrum of PDI **3**. The inset shows the molecular structure of PDI **3** with the assigned protons and carbons. Figure S2 shows the full ^{1}H, ^{13}C HMBC spectrum. B) Expansion of the stacked ^{1}H NMR spectra of 1,7-isomer PDI **11** (top) and 1,12-isomer PDI **7** (bottom).

The above detailed 2D NMR study unequivocally proves that the applied oxidative chemistry to acquire dihydroxylated PDI **2**, indeed results in 1,12-dialkoxy PDI regioisomers after alkylation. Note that this 1,12-assignment is in contradiction with reported 1,7-assignments (that were based solely on ^{1}H NMR spectra) for PDIs that have been prepared using a procedure similar to that delineated here,[63,64] but that the 1,12-assignment is in line with regioisomer assignments as reported for hydroxylated violanthrones.[58] A comparative synthesis of a 1,7-substituted PDI and its 1,12-isomer (see the Supporting Information) provides further evidence for the assignment of the 1,12-substitution topology for PDIs prepared by our procedure. Figure 2b shows the stacked ^{1}H NMR spectra of the 1,7- and 1,12-substituted regioisomers of di-*n*-octyl-substituted PDIs **11** and **7**, respectively. The resonance peaks corresponding to protons H_a in the aromatic region of PDI **11** shift significantly downfield through intramolecular hydrogen-bonding of H_a with the adjacent oxygen atom in the 1,7-subsitution topology. In contrast, the corresponding H_a proton signals in PDI **7** are shifted more upfield, presumably because no intramolecular hydrogen bonding can take place in this 1,12-substituted PDI. Moreover, PDI **11** shows an expected triplet for protons H_g at circa 4.3 ppm, whereas the restricted rotation of the alkoxy substituents in PDI **7** results in a broad peak for these protons (Figure S6). This loss of clear multiplicity for protons H_g is a feature of all 1,12-substituted PDIs studied in the paper.

The bay-substituted PDIs **3**, **4** and **6** were studied by UV/Vis and fluorescence spectroscopy in their molecularly dissolved state in anhydrous dimethyl sulfoxide (DMSO). This solvent was chosen to ensure complete solubility for the doubly charged PDI **7**. Non-bay-substituted PDI **1** is notably less soluble than PDIs **3**–**7** and tends to aggregate at higher concentrations in DMSO. Gratifyingly, PDI **1** was sufficiently soluble in anhydrous tetrahydrofuran (THF) to enable optical measurements at the desired concentration. Table 1 shows the maximum absorption and emission wavelengths, including the extinction coefficient and the quantum yield, of non-bay- and 1,12-bay-substituted PDIs **1**, **3**, **4** and **6** as derived from the UV/Vis and fluorescence spectroscopy studies. The absorption spectra of PDIs bearing a 1,12-substitution topology clearly show a bathochromic shift, broadening of the lowest energy absorption band and thus a loss of sharp vibronic progressions as compared with parent PDI **1** (Figure S7). The latter effect is generally attributed to an out-of-plane distortion of the perylene ring system because of the sterically encumbered substituent groups.[65,66] The overall bathochromic shift of the maximum absorption wavelength is due to the π-donating effect of the oxygen substituents on the perylene ring system.[52] The fluorescence spectra of 1,12-bay-substituted PDIs are a mirror image of their corresponding absorption spectra (Figure 3a),

Table 1. Optical characteristics of PDI derivatives **1**, **3**, **4** and **6** in THF (for **1**) and DMSO (for **3**, **4** and **6**) and in H_2O.

	UV/Vis absorption λ [nm] (ε [10^3 M^{-1} cm^{-1}])		Fluorescence λ_{max} [nm] (ϕ_{PL} [%])[a]	
	THF or DMSO	H_2O	THF or DMSO	H_2O
1	430 (9.1); 455 (20.1); 485 (46.8); 520 (74.0)	–[b]	529; 570; 617 (71)	–[b]
3	400 (9.5); 417 (11.1); 547 (27.2); 582 (36.2)	418 (4.6); 547 (11.9); 585 (9.8)	627 (79)	667; 778 (2)
4	396 (7.1); 416 (9.2); 546 (26.4); 583 (37.1)	423 (4.4); 540 (13.7); 606 (5.5)	628 (80)	718 (0)
6	396 (6.6); 417 (8.5); 546 (24.8); 585 (36.8)	424 (3.5); 556 (11.3); 607 (6.1)	625 (82)	641 (0)

[a] *N*,*N*′-Bis(pentylhexyl)perylene-3,4:9,10-tetracarboxylic diimide ($\phi = 0.99$) in methylene dichloride was used as a reference. [b] PDI **1** is insoluble in H_2O and hence precipitated at 1.5×10^{-5} M.

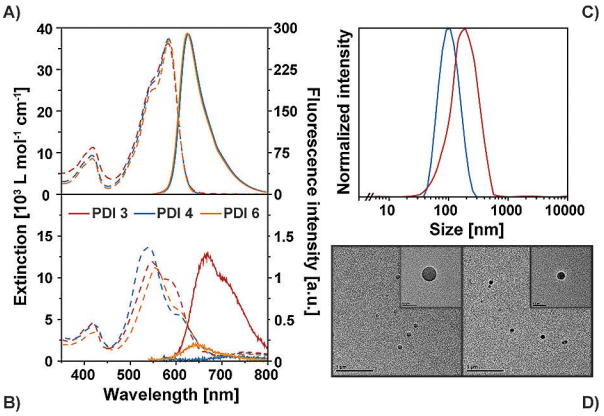

Figure 3. UV/Vis absorption spectra (dashed lines) and corresponding fluorescence spectra (solid lines) of PDI **3**, **4** and **6** in A) DMSO and B) water ($c = 1.5 \times 10^{-5}$ M, $\lambda_{exc} = 530$ nm). C) DLS data indicating diameters of nanoparticles formed by PDI **3** and **4** in water, and D) TEM images of PDI **3** (left) and **4** (right) in water ($c = 1.5 \times 10^{-5}$ M, scale bar: 1 μm, insets: magnified TEM image of the same sample, scale bar: 200 nm).

including the loss of vibronic fine structure accompanied by a relatively large Stokes shift as compared with PDI **1**. The distorted planarity of the perylene ring system additionally contributes to a large bathochromic shift of ca. 100 nm. Quantum yields of ca. 70–80% were measured for all PDI derivatives, independent of the substituents and spectral shapes (Table 1).

Nano-sized assemblies of the PDIs were prepared through reprecipitation in aqueous media.[67] Rapid injection of a DMSO stock solution, containing molecularly dissolved PDI, into filter-sterilised demi water resulted in self-assembled architectures for all PDIs bearing a bay substitution topology. PDI **1** did not form stable self-assembled architectures, but instead formed clearly visible and much larger aggregates (i.e., precipitates) in aqueous solution, also at low concentrations, preventing determination of its optical properties in water. The hypsochromic shift of the absorption maxima of 1,12-bay-substituted PDIs through reversal of the vibronic transitions revealed the formation of H-type π–π stacks,[68,69] which is accompanied by a distinct overall drop in absorption intensity (Figure 3b). Whereas vibronic structure blurring was already observed in organic solvent because of core planarity distortion, a significant drop in overall fluorescence intensity and quantum yield is typically attributed to intermolecular π–π interactions. Even though PDIs are known for their nonradiative relaxation from their excited-state upon polarity induced face-to-face interactions, these bay-substituted PDI derivatives show a large Stokes shift of approximately 100 nm and a bathochromically shifted fluorescence spectrum.

The morphological characteristics of the formed architectures were determined by dynamic light scattering (DLS) and transmission electron microscopy (TEM). DLS analysis showed a strong scattering correlation of PDI **3** and **4** (Figure S8). Fits of the scattering intensity distribution revealed hydrodynamic radii of 83 and 48 nm, respectively (Figure 3c), which are consistent with the observations in TEM images (Figure 3d). Intuitively, the larger particle size of PDI **3** could be explained by the hydrophobicity of the side-chains. Moreover, the drop-casted particles were spherical with a fairly monodisperse distribution. In contrast to PDIs **3** and **4**, neither scattering correlation nor electron microscopic visualisation of cationic PDI **6** could be achieved, suggesting the absence of large aggregates. Whereas the optical data of PDI **6** shows signs of self-assembly, we envision the formation of only small aggregates. The deviating behaviour for PDI **6** is likely due to charge repulsive forces, as has been observed for other polar PDI derivatives.[32] In summary, these novel PDI derivatives show an electronic S_0–S_1 transition resulting in strong absorption in the visible region between 500 and 650 nm in both monomeric and self-assembled state, which makes them suitable for fluorescence microscopy. Moreover, they display bathochromically shifted fluorescence spectra, as compared with non-bay-substituted perylenes.

A challenge in bioimaging to date is to find nontoxic fluorophores of small size and high brightness that operate beyond the optical spectral window of biomatter. From this perspective, all three 1,12-bay-substituted perylene derivatives exhibit interesting physical properties, with PDI **6** being most interesting for bioimaging applications because of its cationic amphiphilic nature, which potentially favours cellular uptake. The potential of PDI **6** as bioimaging probe was investigated by first studying its interaction with artificial lipid bilayers. Therefore, a 5 μM aqueous solution of PDI **6** was incubated in the presence of giant unilamellar vesicles (GUVs) prepared from dipalmitoylphosphatidylcholine (DPPC) by using a standard reverse-phase evaporation method. The resulting fluorescence emission spectrum showed a maximum emission wavelength at 616 nm similar to the maximum observed for this perylene derivative in DMSO, and hypsochromically shifted as compared with the fluorescence in aqueous solution (Figure 3b). This effect indicates that, in the presence of GUVs, PDI **6** is surrounded by a

less polar environment than pure water, and is presumably incorporated in the lipid bilayer (Figure 4a). Moreover, the increased overall perylene fluorescence of the GUVs led us to hypothesise that the molecules are incorporated into the lipid bilayer in monomeric form. Results from temperature-dependent fluorescence studies strengthen this hypothesis as the perylene fluorescence was observed to increase at temperatures above the DPPC transition temperature of 41 °C (Figure 4a). Dye incorporation most likely occurs through insertion of the apolar perylene moiety into the lipid bilayer, whereas the polar heads are exposed to the outer environment along with the polar lipid headgroups.[70] Fluorescence microscopy images show highly fluorescent GUVs after excitation of PDI **6**, and confocal laser scanning microscopy (CLSM) images strongly suggest that the fluorescence originates from the lipid bilayer, corroborating the hypothesis of incorporation of PDI **6** into the lipid bilayer (Figure 4b–d).

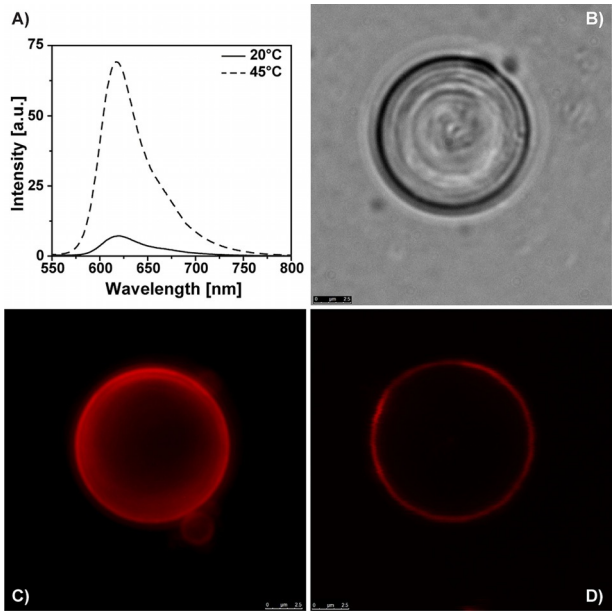

Figure 4. A) Fluorescence spectra of GUV's (DPPC) incubated with a 5 μM solution of PDI **6** in water at two different temperatures ($c = 1.5 \times 10^{-5}$ M, $\lambda_{exc} = 530$ nm). B) Brightfield, C) fluorescence and D) confocal laser scanning microscopy images of GUV's (DPPC) incubated with a 5 μM solution of PDI **6**.

Next, the optical properties as well as the aggregation state of PDI **6** were studied in phosphate buffered saline (PBS), having a higher ionic strength than pure water. The absorption spectra of PDI **6** in water and PBS were similar (Figure S9a), indicating an aggregated state of PDI **6** in both solutions. Interestingly, a slight drop in intensity of the electronic S_0–S_1 transition can be observed in PBS, which is nevertheless indicative of differences. Figures S9b and S9c show the scattering correlation and the fitted hydrodynamic diameter, of around 275 nm, of PDI **6** in PBS. This DLS analysis shows that the doubly charged perylene derivative is assembled in larger nanostructures in PBS, in contrast to water, most likely because of the ionic strength of the buffer.

Cellular uptake studies were performed to study the potential of PDI **6** as an off-on fluorescent lipid probe or organelle stain for bioimaging applications.[71,72] For these applications, the toxicity of a probe needs to be kept to a minimum; thus, the cellular toxicity of PDI **6** was measured with a MTT-cell activity assay. PDI **6** was observed to be nontoxic at probe concentrations up to the highest test concentration (100 μM) after incubation for two hours (Figure S10). Based on these findings, a 5 μM concentration was chosen for all cellular incubation studies to ensure good fluorescence signal while minimising toxicity.

Hela cells were incubated with PDI **6** for two hours and analysed by CLSM after washing. Cellular uptake of this cationic probe was clearly observed under the aforementioned conditions (Figure 5) compared with the negative control in which

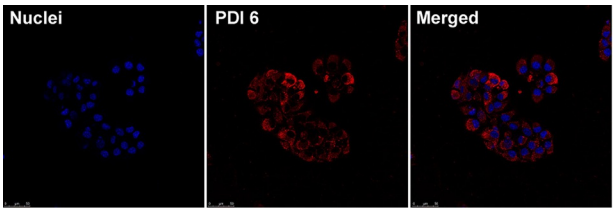

Figure 5. CLSM images of Hela cells after two hours incubation with a 5 μM solution of PDI **6** (nuclei are stained with Hoechst dye, scale bar: 50 μm).

no probe was administered (Figure S11). Subsequently, the cellular uptake process was monitored by incubating Hela cells with the probe under the same conditions, followed by time-course analysis by CLSM (Figure S12). Interestingly, immediately upon administration, the probe was observed to accumulate at the plasma membrane, which reached saturation within 5 minutes incubation time. The first signs of cellular uptake were then seen after 15 minutes incubation in the form of small vesicular structures at the inside of the plasma membrane. These small vesicular structures then appeared to translocate further into the cell, apparently towards the Golgi apparatus as they eventually surround the nucleus after about 30 minutes, post-administration. This distribution pattern indicates cellular uptake of the probe through an endocytic pathway. It is important to note here that the cells were not washed prior to imaging and that the PDI nanostructures were not visible in the surrounding media, thus only become highly fluorescent upon interaction with the cellular membrane.

Co-localisation studies on perylene probe PDI **6**—two staining compartments involved in endocytic routes and the third stains parts of the cytoskeleton (Figure 6)—revealed that the perylene probe did not interact with actin in the cytoskeleton nor did they localise in the endoplasmatic reticulum (ER). The lysosomal tracker shows a high correlation and, thus, the nature of the observed vesicular structures can be assigned as lysosomes. The lack of strong co-localisation with the ER as well as high lysosomal co-localisation are not uncommon for endocytic pathways. Nanostructures that are endocytically internalised are commonly transported to lysosomes.[73] However, whereas nanosized architectures are usually internalised as a

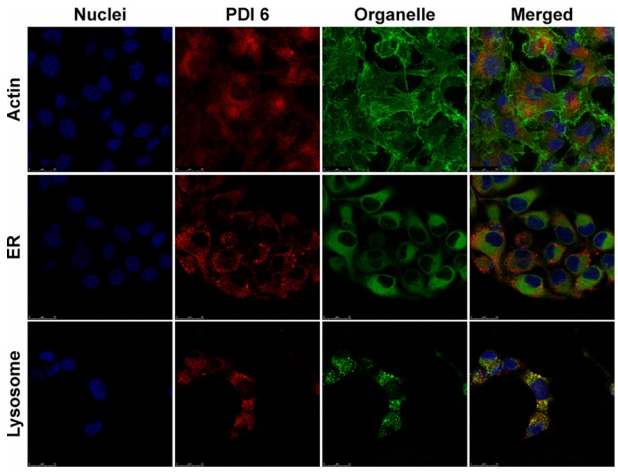

Figure 6. CLSM images of Hela cells after two hours incubation with a 5 μM solution of PDI **6** co-stained with different organelle markers, showing the lack of co-localisation with actin and ER markers while strong co-localization with a lysosomal marker is shown (nuclei are stained with DAPI in fixed cells and with Hoechst in live cells, scale bar: 50 μm).

whole inside the lysosome where the digestive processes occur, it is hypothesised that PDI **6** stains hydrophobic compartments by merging with the membrane. Indications for the insertion of probe into the fluid lipid membrane were found by performing full wavelength fluorescence measurements on the cells. Figure 7 shows the emission spectrum of cells incubated with 5 μM of PDI **6** for two hours as well as the spectra

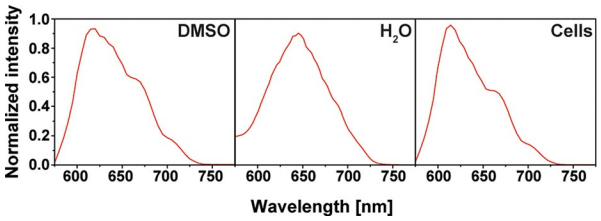

Figure 7. Normalised fluorescence spectra of 5 μM solution of PDI **6** in DMSO and water and Hela cells incubated with 5 μM solution of PDI **6** as measured by CLSM, respectively.

of the probe in DMSO and water at similar concentrations as measured by CLSM. It can be clearly seen that the cells show an emission spectra that more closely resembles the emission spectra of the probe in DMSO and in the GUVs, as similar maximum emission wavelengths and vibronic fine structure can be observed, and clearly deviates from the emission spectrum recorded in water. Therefore, we envision a cellular uptake process through merging of the nanostructure with the fluid lipid membrane through which the monomers are incorporated into the lipophilic environment. The monomerisation of the probe in the hydrophobic membrane matrix concomitantly leads to activation of fluorescence of the perylene ring system and clear visualisation of cellular membranes.

Conclusions

We have shown an efficient and facile synthetic entry into exclusively 1,12-bay-substituted perylene diimides (PDIs) through a direct hydroxylation reaction. Accordingly, this substitution pattern is accessed without the need for sequential halogenation and dehalogenation reactions. Further derivatisation of the two hydroxyl groups allows a wide range of substituents to be to potentially introduced through straightforward O-alkylation and leads to PDIs that display an increased solubility in organic solvents. The 1,12-substitution of the PDIs results in a bathochromic shift of the optical properties of the compounds, which is favourable for imaging applications. Upon introducing hydrophilic groups, the PDIs can be regarded as a new class of gemini surfactants having unprecedented optical and self-assembly properties. For example, GUVs could be subjected to nonfluorescence aggregates of a cationic PDI derivative bearing two quaternary ammonium moieties and the lipophilic bilayer of the GUVs turned highly fluorescent immediately after administration. Fluorescence measurements showed the incorporation of the PDI derivatives in the lipophilic bilayer. Subsequent cellular studies showed similar results, as PDI fluorescence was strongly observed in cellular membranes and cellular uptake was observed only 15 minutes after administration. Co-localization studies and full wavelength cell fluorescence measurements revealed that the quenched aggregates merge with cellular membranes. Given the concomitant monomerisation and, hence, fluorescence recovery of the perylene ring system, this synthetically easily accessible PDI amphiphile is functioning as an off-on fluorescent probe for imaging lipid bilayers. Moreover, this probe can also be envisioned to function as a potential trackable platform to anchor bio-active compounds into membrane-containing cellular compartments.

Experimental Section

General remarks

Details on used chemicals and equipment can be found in the Supporting Information.

Dynamic light scattering

DLS experiments were performed with a Malvern Instruments Limited Zetasizer μV (model: ZMV2000). The incident beam was produced with a HeNe laser operating at 632 nm. Samples were measured unfiltered at 1.5×10^{-5} M.

Transmission electron microscopy

Visualisation by TEM was performed with a Technai G2 Sphera by FEI operating at an acceleration voltage of 80 kV. Samples were prepared by drop-casting a 1.5×10^{-5} M aqueous PDI solution on a carbon film on a 400 square mesh copper grid and dried for one minute.

Particle formation

Nanosized architectures were prepared from unimolecular building blocks by means of reprecipitation. This includes rapid injection of

15 μL of a 1×10^{-3} M PDI stock solution dissolved in anhydrous dimethyl sulfoxide (≥99.9%) into 1 mL filter sterilised demineralised water followed by manual stirring, yielding a 1.5×10^{-5} M nanoparticle solution.

Optical measurements

UV/Vis absorption spectra were measured with a Jasco V-650 spectrophotometer equipped with a PerkinElmer PTP-1 Peltier temperature control system. The spectra were measured in quartz cuvettes and extinction coefficients were calculated from Beer–Lambert's law. Fluorescence spectra were recorded with a Varian Cary Eclipse fluorescence spectrophotometer. Fluorescence quantum yields (ϕ) were calculated from the integrated intensity under the emission band (I) using Equation (1), where OD is the optical density of the solution at the excitation wavelength and n is the refractive index; *N*,*N*′-bis(pentylhexyl)perylene-3,4:9,10-teteracarboxylic acid diimide ($\phi=0.99$) in methylene dichloride was used as reference.

$$\phi = \phi_r \frac{I}{I_r}\frac{OD_r}{OD}\frac{n^2}{n_r^2} \quad (1)$$

Liposomes

Dipalmitoylphosphatidylcholine lipids (DPPC, 10 mg) were dissolved in a solution of chloroform (5 mL) containing 5% methanol. The aqueous phase (5 mL of water) was carefully added along the flask walls. The organic solvent was removed in a rotary evaporator at 40 °C at 40 rpm. After drying, an opalescent fluid was obtained with a volume of approximately 4.5 mL containing a mixture of heterogeneous DPPC liposomes. Liposomes were characterised by brightfield and fluorescence microscopy with a Zeiss Axio Observer D1 equipped with an LD Plan-NeoFluar 40×/0.6 Korr Ph 2 lens. A HE DsRed reflector (Exc: 538–562; Em: 570–640) was used to image PDI **6**. CLSM measurements were performed in a similar fashion as for the cells.

Confocal microscopy

HeLa cells were seeded in eight-well uncoated glass-bottom plates (30000 cells per well) and cultured for 24 h at 37 °C/5% CO_2 in Dulbecco's modified Eagle medium (DMEM) supplemented with 10% fetal bovine serum (FBS) and 1% penicillin-streptomycin (Pen/Strep). Prior to imaging, the medium was removed and replaced by a 5 μM PDI **6** solution in cell culture medium without phenol red. After two hours incubation, the solution was removed, the cells were washed with PBS and fresh DMEM was added. The cells were imaged with a Leica TCS SP5 AOBS equipped with an HCX PL APO CS ×63/1.2 NA water-immersion lens and a temperature-controlled incubation chamber maintained at 37 °C. PDI **6** was excited with a white-light laser at 530 nm with the pinhole set to one airy unit. The detection range was set to 550–750 nm. The organelle markers (Alexa Fluor 680 Phalloidin, ER-tracker Green and LysoTracker Green DND-26) were used according to the manufacturers' protocol in the co-localisation studies. For the actin co-stained samples, the cells were fixed with paraformaldehyde in PBS for 10 min at room temperature. The microscopy images were analysed using Leica Application Suite X.

Supporting Information

Details on used chemicals and equipment, synthetic procedures and characterisation, DLS, UV/Vis absorption and emission spectra, MTT-cell activity assay and CLSM supporting figures can be found in the Supporting Information.

Acknowledgements

The research was supported by funding from HTSM through STW grant 12859-FluNanoPart and the Netherlands Organization for Scientific Research (NWO) via Gravity program 024.001.035, VICI grant 016.150.366 and ECHO grant 711.013.015.

Conflict of interest

The authors declare no conflict of interest.

Keywords: bioimaging · dyes/pigments · nanoparticles · surfactants · supramolecular chemistry

[1] C. Li, H. Wonneberger, *Adv. Mater.* **2012**, *24*, 613–636.
[2] F. Würthner, C. R. Saha-Möller, B. Fimmel, S. Ogi, P. Leowanawat, D. Schmidt, *Chem. Rev.* **2016**, *116*, 962–1052.
[3] S. Chen, P. Slattum, C. Wang, L. Zang, *Chem. Rev.* **2015**, *115*, 11967–11998.
[4] E. Lang, R. Hildner, H. Engelke, P. Osswald, F. Würthner, J. Köhler, *ChemPhysChem* **2007**, *8*, 1487–1496.
[5] K. Peneva, G. Mihov, F. Nolde, S. Rocha, J. Hotta, K. Braeckmans, J. Hofkens, H. Uji-i, A. Herrmann, K. Müllen, *Angew. Chem. Int. Ed.* **2008**, *47*, 3372–3375; *Angew. Chem.* **2008**, *120*, 3420–3423.
[6] M. Davies, C. Jung, P. Wallis, T. Schnitzler, C. Li, K. Müllen, C. Bräuchle, *ChemPhysChem* **2011**, *12*, 1588–1595.
[7] T. Heek, C. Fasting, C. Rest, X. Zhang, F. Würthner, R. Haag, *Chem. Commun.* **2010**, *46*, 1884–1886.
[8] S. K. Yang, X. Shi, S. Park, S. Doganay, T. Ha, S. C. Zimmerman, *J. Am. Chem. Soc.* **2011**, *133*, 9964–9967.
[9] J. Schill, A. P. H. J. Schenning, L. Brunsveld, *Macromol. Rapid Commun.* **2015**, *36*, 1306–1321.
[10] M. Yin, J. Shen, G. O. Pflugfelder, K. Müllen, *J. Am. Chem. Soc.* **2008**, *130*, 7806–7807.
[11] T. Ribeiro, S. Raja, A. S. Rodrigues, F. Fernandes, C. Baleizão, J. P. S. Farinha, *Dyes Pigm.* **2014**, *110*, 227–234.
[12] D. Aigner, R. I. Dmitriev, S. M. Borisov, D. B. Papkovsky, I. Klimant, *J. Mater. Chem. B* **2014**, *2*, 6792–6801.
[13] K. Trofymchuk, A. Reisch, I. Shulov, Y. Mély, A. S. Klymchenko, *Nanoscale* **2014**, *6*, 12934–12942.
[14] S. You, Q. Cai, Y. Zheng, B. He, J. Shen, W. Yang, M. Yin, *ACS Appl. Mater. Interfaces* **2014**, *6*, 16327–16334.
[15] P. Singh, L. S. Mittal, V. Vanita, R. Kumar, G. Bhargava, A. Walia, S. Kumar, *Chem. Commun.* **2014**, *50*, 13994–13997.
[16] Q. Fan, K. Cheng, Z. Yang, R. Zhang, M. Yang, X. Hu, X. Ma, L. Bu, X. Lu, X. Xiong, W. Huang, H. Zhao, Z. Cheng, *Adv. Mater.* **2015**, *27*, 843–847.
[17] K. Liu, Z. Xu, M. Yin, *Prog. Polym. Sci.* **2015**, *46*, 25–54.
[18] A. Jana, L. Bai, X. Li, H. Ågren, Y. Zhao, *ACS Appl. Mater. Interfaces* **2016**, *8*, 2336–2347.
[19] H. Tan, H. Liu, Y. Liu, W. Duan, X. Yi, Y. Wu, H. Zhao, L. Bai, *J. Biomater. Sci. Polym. Ed.* **2016**, *27*, 455–471.
[20] T. Heek, C. Kühne, H. Depner, K. Achazi, J. Dernedde, R. Haag, *Bioconjugate Chem.* **2016**, *27*, 727–736.
[21] D. Görl, X. Zhang, F. Würthner, *Angew. Chem. Int. Ed.* **2012**, *51*, 6328–6348; *Angew. Chem.* **2012**, *124*, 6434–6455.
[22] J. Gershberg, M. R. Stojković, M. Škugor, S. Tomić, T. H. Rehm, S. Rehm, C. R. Saha-Möller, I. Piantanida, F. Würthner, *Chem. Eur. J.* **2015**, *21*, 7886–7895.
[23] M. Sun, K. Müllen, M. Yin, *Chem. Soc. Rev.* **2016**, *45*, 1513–1528.

[24] M. Gsänger, J. H. Oh, M. Könemann, H. W. Höffken, A.-M. Krause, Z. Bao, F. Würthner, *Angew. Chem. Int. Ed.* **2010**, *49*, 740 – 743; *Angew. Chem.* **2010**, *122*, 752 – 755.
[25] T. T. Clikeman, E. V. Bukovsky, X.-B. Wang, Y.-S. Chen, G. Rumbles, S. H. Strauss, O. V. Boltalina, *Eur. J. Org. Chem.* **2015**, 6641 – 6654.
[26] H. Langhals, *Heterocycles* **1995**, *40*, 477.
[27] L. D. Wescott, D. L. Mattern, *J. Org. Chem.* **2003**, *68*, 10058 – 10066.
[28] Y. Nagao, *Prog. Org. Coat.* **1997**, *31*, 43 – 49.
[29] K. Balakrishnan, A. Datar, T. Naddo, J. Huang, R. Oitker, M. Yen, J. Zhao, L. Zang, *J. Am. Chem. Soc.* **2006**, *128*, 7390 – 7398.
[30] F. May, V. Marcon, M. R. Hansen, F. Grozema, D. Andrienko, *J. Mater. Chem.* **2011**, *21*, 9538 – 9545.
[31] X. Zhang, D. Görl, V. Stepanenko, F. Würthner, *Angew. Chem. Int. Ed.* **2014**, *53*, 1270 – 1274; *Angew. Chem.* **2014**, *126*, 1294 – 1298.
[32] J. Schill, L.-G. Milroy, J. A. M. Lugger, A. P. H. J. Schenning, L. Brunsveld, *ChemistryOpen* **2017**, *6*, 266 – 272.
[33] F. Würthner, *Pure Appl. Chem.* **2006**, *78*, 2341 – 2349.
[34] S. Nakazono, S. Easwaramoorthi, D. Kim, H. Shinokubo, A. Osuka, *Org. Lett.* **2009**, *11*, 5426 – 5429.
[35] C. Huang, S. Barlow, S. R. Marder, *J. Org. Chem.* **2011**, *76*, 2386 – 2407.
[36] G. Battagliarin, Y. Zhao, C. Li, K. Müllen, *Org. Lett.* **2011**, *13*, 3399 – 3401.
[37] R. Schmidt, J. H. Oh, Y.-S. Sun, M. Deppisch, A.-M. Krause, K. Radacki, H. Braunschweig, M. Könemann, P. Erk, Z. Bao, F. Würthner, *J. Am. Chem. Soc.* **2009**, *131*, 6215 – 6228.
[38] X. Zhang, C. Zhan, X. Zhang, J. Yao, *Tetrahedron* **2013**, *69*, 8155 – 8160.
[39] F. Würthner, *Chem. Commun.* **2004**, 1564 – 1579.
[40] W. Qiu, S. Chen, X. Sun, Y. Liu, D. Zhu, *Org. Lett.* **2006**, *8*, 867 – 870.
[41] Z. An, S. A. Odom, R. F. Kelley, C. Huang, X. Zhang, S. Barlow, L. A. Padilha, J. Fu, S. Webster, D. J. Hagan, E. W. Van Stryland, M. R. Wasielewski, S. R. Marder, *J. Phys. Chem. A* **2009**, *113*, 5585 – 5593.
[42] S. Dey, A. Efimov, H. Lemmetyinen, *Eur. J. Org. Chem.* **2012**, 2367 – 2374.
[43] M.-J. Lin, Á. J. Jiménez, C. Burschka, F. Würthner, *Chem. Commun.* **2012**, *48*, 12050 – 12052.
[44] P. Rajasingh, R. Cohen, E. Shirman, L. J. W. Shimon, B. Rybtchinski, *J. Org. Chem.* **2007**, *72*, 5973 – 5979.
[45] R. K. Dubey, A. Efimov, H. Lemmetyinen, *Chem. Mater.* **2011**, *23*, 778 – 788.
[46] Y. Li, Z. Qing, Y. Yu, T. Liu, R. Jiang, Y. Li, *Chem. Asian J.* **2012**, *7*, 1934 – 1939.
[47] Z. Lu, X. Zhang, C. Zhan, B. Jiang, X. Zhang, L. Chen, J. Yao, *Phys. Chem. Chem. Phys.* **2013**, *15*, 11375 – 11385.
[48] C.-Y. Chan, Y.-C. Wong, H.-L. Wong, M.-Y. Chan, V. W.-W. Yam, *J. Mater. Chem. C* **2014**, *2*, 7656 – 7665.
[49] F. Würthner, V. Stepanenko, Z. Chen, C. R. Saha-Möller, N. Kocher, D. Stalke, *J. Org. Chem.* **2004**, *69*, 7933 – 7939.
[50] N. V. Handa, K. D. Mendoza, L. D. Shirtcliff, *Org. Lett.* **2011**, *13*, 4724 – 4727.
[51] P. Osswald, F. Würthner, *J. Am. Chem. Soc.* **2007**, *129*, 14319 – 14326.
[52] B. Pagoaga, O. Mongin, M. Caselli, D. Vanossi, F. Momicchioli, M. Blanchard-Desce, G. Lemercier, N. Hoffmann, G. Ponterini, *Phys. Chem. Chem. Phys.* **2016**, *18*, 4924 – 4941.
[53] P. Leowanawat, A. Nowak-Król, F. Würthner, *Org. Chem. Front.* **2016**, *3*, 537 – 544.
[54] H. Qian, Z. Wang, W. Yue, D. Zhu, *J. Am. Chem. Soc.* **2007**, *129*, 10664 – 10665.
[55] Y. Shi, H. Qian, Y. Li, W. Yue, Z. Wang, *Org. Lett.* **2008**, *10*, 2337 – 2340.
[56] Y. Zhen, H. Qian, J. Xiang, J. Qu, Z. Wang, *Org. Lett.* **2009**, *11*, 3084 – 3087.
[57] B. Pagoaga, L. Giraudet, N. Hoffmann, *Eur. J. Org. Chem.* **2014**, 5178 – 5195.
[58] M.-M. Shi, Y. Chen, Y.-X. Nan, J. Ling, L.-J. Zuo, W.-M. Qiu, M. Wang, H.-Z. Chen, *J. Phys. Chem. B* **2011**, *115*, 618 – 623.
[59] F. M. Menger, C. A. Littau, *J. Am. Chem. Soc.* **1993**, *115*, 10083 – 10090.
[60] H. Langhals, S. Demmig, T. Potrawa, *J. Prakt. Chem.* **1991**, *333*, 733 – 748.
[61] Y. Nagao, T. Misono, *Bull. Chem. Soc. Jpn.* **1981**, *54*, 1191 – 1194.
[62] N. C. Gonnella, *LC-NMR: Expanding the Limits of Structure Elucidation*, CRC, Boca Raton, **2013**.
[63] L. Perrin, P. Hudhomme, *Eur. J. Org. Chem.* **2011**, 5427 – 5440.
[64] L. Zhang, L. Wang, G. Zhang, J. Yu, X. Cai, M. Teng, Y. Wu, *Chin. J. Chem.* **2012**, *30*, 2823 – 2826.
[65] J. Hofkens, T. Vosch, M. Maus, F. Köhn, M. Cotlet, T. Weil, A. Herrmann, K. Müllen, F. C. De Schryver, *Chem. Phys. Lett.* **2001**, *333*, 255 – 263.
[66] E. Fron, G. Schweitzer, P. Osswald, F. Würthner, P. Marsal, D. Beljonne, K. Müllen, F. C. D. Schryver, M. V. der Auweraer, *Photochem. Photobiol. Sci.* **2008**, *7*, 1509 – 1521.
[67] H. Kasai, H. S. Nalwa, H. Oikawa, S. Okada, H. Matsuda, N. Minami, A. Kakuta, K. Ono, A. Mukoh, H. Nakanishi, *Jpn. J. Appl. Phys.* **1992**, *31*, L1132 – L1134.
[68] T. Weil, M. A. Abdalla, C. Jatzke, J. Hengstler, K. Müllen, *Biomacromolecules* **2005**, *6*, 68 – 79.
[69] S. Yagai, T. Seki, T. Karatsu, A. Kitamura, F. Würthner, *Angew. Chem. Int. Ed.* **2008**, *47*, 3367 – 3371; *Angew. Chem.* **2008**, *120*, 3415 – 3419.
[70] K. Jacobson, D. Papahadjopoulos, *Biophys. J.* **1976**, *16*, 549 – 560.
[71] T. Heek, J. Nikolaus, R. Schwarzer, C. Fasting, P. Welker, K. Licha, A. Herrmann, R. Haag, *Bioconjugate Chem.* **2013**, *24*, 153 – 158.
[72] M. Franceschin, C. Bombelli, S. Borioni, G. Bozzuto, S. Eleuteri, G. Mancini, A. Molinari, A. Bianco, *New J. Chem.* **2013**, *37*, 2166 – 2173.
[73] S. Zhang, H. Gao, G. Bao, *ACS Nano* **2015**, *9*, 8655 – 8671.

Manuscript received: February 28, 2018
Revised manuscript received: March 20, 2018
Accepted manuscript online: March 22, 2018
Version of record online: May 3, 2018

